

Original Research



Machine-learning aided *in situ* drug sensitivity screening predicts treatment outcomes in ovarian PDX tumors

Max J. Cotler^{a,b,1}, Khalil B. Ramadi^{a,b,1}, Xiaonan Hou^c, Elena Christodoulou^a, Sebastian Ahn^d, Ashvin Bashyam^{a,f}, Huiming Ding^a, Melissa Larson^e, Ann L. Oberg^e, Charles Whittaker^a, Oliver Jonas^{a,d}, Scott H. Kaufmann^{c,g}, S. John Weroha^{c,g}, Michael J. Cima^{a,h,*}

^a The David H. Koch Institute for Integrative Cancer Research, Massachusetts Institute of Technology, Cambridge, MA 02139, USA

^b Harvard-MIT Program in Health Sciences and Technology, Massachusetts Institute of Technology, Cambridge, MA 02139, USA

^c Department of Oncology, Mayo Clinic, Rochester, MN 55905, USA

^d Department of Radiology, Brigham and Women's Hospital, Boston, MA 02115, USA

^e Division of Computational Biology, Department of Quantitative Health Sciences, Mayo Clinic, Rochester, MN 55905, USA

^f Department of Electrical Engineering and Computer Science, Massachusetts Institute of Technology, Cambridge, MA 02139, USA

^g Department of Molecular Pharmacology and Experimental Therapeutics, Mayo Clinic, Rochester, MN 55905, USA

^h Department of Materials Science and Engineering, Massachusetts Institute of Technology, Cambridge, MA 02139, USA

ARTICLE INFO

Keywords:

Drug delivery
Ovarian cancer
Personalized medicine
Patient derived xenograft

ABSTRACT

Long-term treatment outcomes for patients with high grade ovarian cancers have not changed despite innovations in therapies. There is no recommended assay for predicting patient response to second-line therapy, thus clinicians must make treatment decisions based on each individual patient. Patient-derived xenograft (PDX) tumors have been shown to predict drug sensitivity in ovarian cancer patients, but the time frame for intraperitoneal (IP) tumor generation, expansion, and drug screening is beyond that for tumor recurrence and platinum resistance to occur, thus results do not have clinical utility. We describe a drug sensitivity screening assay using a drug delivery microdevice implanted for 24 h in subcutaneous (SQ) ovarian PDX tumors to predict treatment outcomes in matched IP PDX tumors in a clinically relevant time frame. The SQ tumor response to local microdose drug exposure was found to be predictive of the growth of matched IP tumors after multi-week systemic therapy using significantly fewer animals (10 SQ vs 206 IP). Multiplexed immunofluorescence image analysis of phenotypic tumor response combined with a machine learning classifier could predict IP treatment outcomes against three second-line cytotoxic therapies with an average AUC of 0.91.

Introduction

Understanding the impact of different drugs on patient-specific tumor progression has far-reaching implications in personalizing therapy. Assigning patients to targeted and cytotoxic therapies currently relies upon genomic technologies and histology, but these techniques have fundamental limitations in guiding treatment, including differences in the number of additional mutations across cancers [1], a lack of validation regarding clinical utility, a disconnect between past molecular aberrations and the constantly-evolving cancer genome [2,3], and

practical barriers to obtaining off-label or investigational agents for patients based on genomic or histologic assays. It is currently estimated that, across cancers, 15% or fewer patients in developed countries receive genome-informed treatment selection, and only 5–8% experience clinical benefit [4,5]. There is no widely-accepted predictive molecular or functional assay for chemotherapy response, and the American Society for Clinical Oncology does not recommend such assays outside of a clinical trial [6]. Oncologists must, therefore, select chemotherapy regimens based on a number of factors that vary by each individual patient.

Abbreviations: PDX, Patient derived xenograft.

* Corresponding author at: The David H. Koch Institute for Integrative Cancer Research, Massachusetts Institute of Technology, Cambridge, MA 02139, USA.

E-mail address: mjcima@mit.edu (M.J. Cima).

¹ These authors contributed equally to this work.

<https://doi.org/10.1016/j.tranon.2022.101427>

Received 6 December 2021; Received in revised form 28 February 2022; Accepted 10 April 2022

Available online 26 April 2022

1936-5233/© 2022 The Authors. Published by Elsevier Inc. This is an open access article under the CC BY-NC-ND license (<http://creativecommons.org/licenses/by-nc-nd/4.0/>).

This lack of a predictive assay is particularly problematic in high-grade ovarian cancers, including serous and others, which remains the deadliest gynecological malignancy in developed countries [7]. The majority of patients who receive first-line treatment of surgical debulking and adjuvant or neoadjuvant taxane platinum (platinum doublet) therapy will achieve remission but over 70% of patients' tumors will relapse as platinum resistant despite advances in surgical technique and therapy administration/cycling [8–13]. Standard second-line cytotoxic chemotherapies, achieve similar response rates of 15–20% and progression free survival rates between 4 and 6 months [9, 14–16]. While genomics and other techniques have identified potentially druggable targets [14], putative candidates for therapy (e.g. *KRAS*, *PIK3CA*) beyond *BRCA1/2* are infrequent and have not lead to widespread clinical benefit [15,17–21]. Recent approvals of PARP inhibitor (PARPi) therapy as maintenance therapy for all patients, including *BRCA1/2* wildtype, without a functional assay for assigning patients to therapy have left clinicians with little guidance. This struggle is seen in multiple malignancies beyond ovarian cancer. Better methods for predicting an individual patient's response to therapy would allow optimization of patient care and minimize the unnecessary burden (toxicity, cost, and time) of current 'trial-and-error' treatment strategies.

Patient-derived xenograft (PDX) models of cancer are a promising tool used in preclinical drug development. Ovarian PDX tumors engrafted intraperitoneally (IP) in immunodeficient mice have been shown to represent the phenotypic and genetic heterogeneity of patient tumors [22–31]. However, use of PDX models to guide clinical therapy in ovarian cancer faces multiple limitations. Tumor engraftment/expansion and complete *in vivo* drug sensitivity testing typically takes 10–15 months due to the need for several rounds of tumor expansion and large animal cohorts for 4-week drug sensitivity testing (>20 mice for a 4-arm study). Patients with platinum resistant or refractory disease will have recurrences <6 months following completion of platinum therapy and, therefore, derive no benefit from PDX studies [16]. Methods to improve the speed of drug sensitivity testing are required to make PDX-enabled predictions, which are known to be accurate, clinically viable treatment planning tools or to provide an alternative to PDXs and genetic profiling.

We have recently developed an implantable microdevice that enables parallel *in vivo* drug sensitivity testing to address some of the challenges outlined above [32–36]. The microdevice contains 18 reservoirs, each filled with a drug micro-dose. Drugs are formulated to diffuse locally at therapeutically relevant concentrations once the device is implanted into a tumor [32]. Tissue surrounding the micro-doses can then be independently analyzed to assess the phenotypic response to each drug without the need for systemic administration. The toxicity risk of the method is very low as only nanogram quantities per drug are used. Moreover, results using this platform correlate with outcomes from systemic drug therapy in multiple tumor models, leading to current clinical study of this approach (NCT04135807, NCT03972228, NCT04399876) [32–35]. A similar device has also been reported with promising results using micro-dose drug injections to predict patient outcomes in sarcoma [37,38]. This platform relies upon an array of 8, 25-gauge needles, which requires a minimum tumor volume of over 600 mm³ and is specific for easily accessible superficial tumors. The implantable microdevice outlined here contains 18 drug reservoirs, only requires 2.73 mm³ of tumor, and is implantable in any tumor that can be reached with a standard biopsy.

Here we demonstrate, for the first time, that a 24 h *in situ* drug sensitivity assay in PDX tumors, when combined with digital immunofluorescence analysis and machine learning (ML) classifiers, can accurately predict systemic treatment outcomes in a clinically relevant time frame (within 3–6 months of surgery and before platinum doublet therapy completion). We hypothesize that accurate predictions of outcomes in IP PDX ovarian tumors, which are predictive of patient outcomes, represents the potential for accurate predictions of patient outcomes using the implant and computational platform. This platform

has the potential to make microdose drug measurements in PDXs a practical tool to advance effective treatments, as well as enable direct drug sensitivity testing in patients' tumors.

Materials and methods

PDX generation and IP engraftment

Fresh tissues from seven patients with ovarian or fallopian tube cancer were collected at the time of primary debulking surgery at Mayo Clinic, Rochester. Written informed consent was obtained from all patients and documented in the electronic medical record. All tissues were coded with a patient heterotransplant (PH) number to protect patient identity in accordance with the Mayo Clinic IRB and in accordance with the Health Insurance Portability and Accountability Act through the Mayo Clinic Ovarian Tumor Repository. Patient characteristics can be seen in Table 1. PDXs were developed by intraperitoneal injection of the donor tumor into female SCID beige mice (C.B.-17/*IcrHsd-Prkdc^{scid}Lyst^{bg}*; Envigo, Indianapolis, IN), and tumors were expanded and cryopreserved (Supplemental Methods, Fig. 1A). IP tumors were injected and engraftment sites were partially dependent on stochastic events. Cryopreserved tumor was then re-engrafted IP or subcutaneously (SQ). Re-engrafted IP PDX tumors were treated with carboplatin-paclitaxel (carbo-taxol) therapy followed by a period of regrowth to eliminate the most sensitive cells before 4 weeks of IP chemotherapy (liposomal doxorubicin, topotecan, paclitaxel, saline).

All studies with human samples were approved by Mayo Clinic Institutional Review Board (IRB) under IRB #09-008768. All animal studies were carried out in accordance with the relevant guideline and regulations of the Mayo Clinic Institutional Animal Care and Use Committee. All methods were performed in accordance with the relevant guidelines and regulations.

IP PDX treatment

Mice with IP PDX tumors greater than 0.3–0.5 cm² in cross-sectional area were randomized and treated with drug or saline control via weekly IP injection over 4 weeks ($n \geq 3$ per group, Paclitaxel 33 mg/kg, Doxorubicin-PEG 2.4 mg/kg, Topotecan 10 mg/kg). Abdominal ultrasound measurements were taken weekly and plotted as the mean tumor

Table 1
Patient characteristics.

	Patient ID	Age at Dx	Stage	Grade and Histology	Platinum Status	Survival (mos.) [†]
1	PH354	60	IIIC	High Grade Serous Primary Peritoneal	Resistant	35
2	PH580	62	IIIA	High Grade Serous Primary Peritoneal	Sensitive	>52
3	PH626	59	IIIC	High Grade Serous Epithelial	Resistant*	13
4	PH704	64	IIIC	High Grade Serous Fallopian Tube	Sensitive	>37
5	PH723	51	IV	High Grade Clear Cell and Undifferentiated Epithelial	Resistant*	10
6	PH756	65	IVB	High Grade Serous Epithelial	Sensitive	>34
7	PH778	62	IIB	High Grade Serous Epithelial	Sensitive	>33

*Platinum refractory with growth during platinum doublet therapy
[†]Survival from date of diagnosis

Ovarian cancer tissue was harvested from patients at the Mayo Clinic undergoing surgical debulking. Banked tissue from 7 patients was used in this study to engraft both IP and SQ PDX tumors in SCID mice. Resistance is defined as patient tumor regrowth within 6 months of completing platinum doublet therapy.

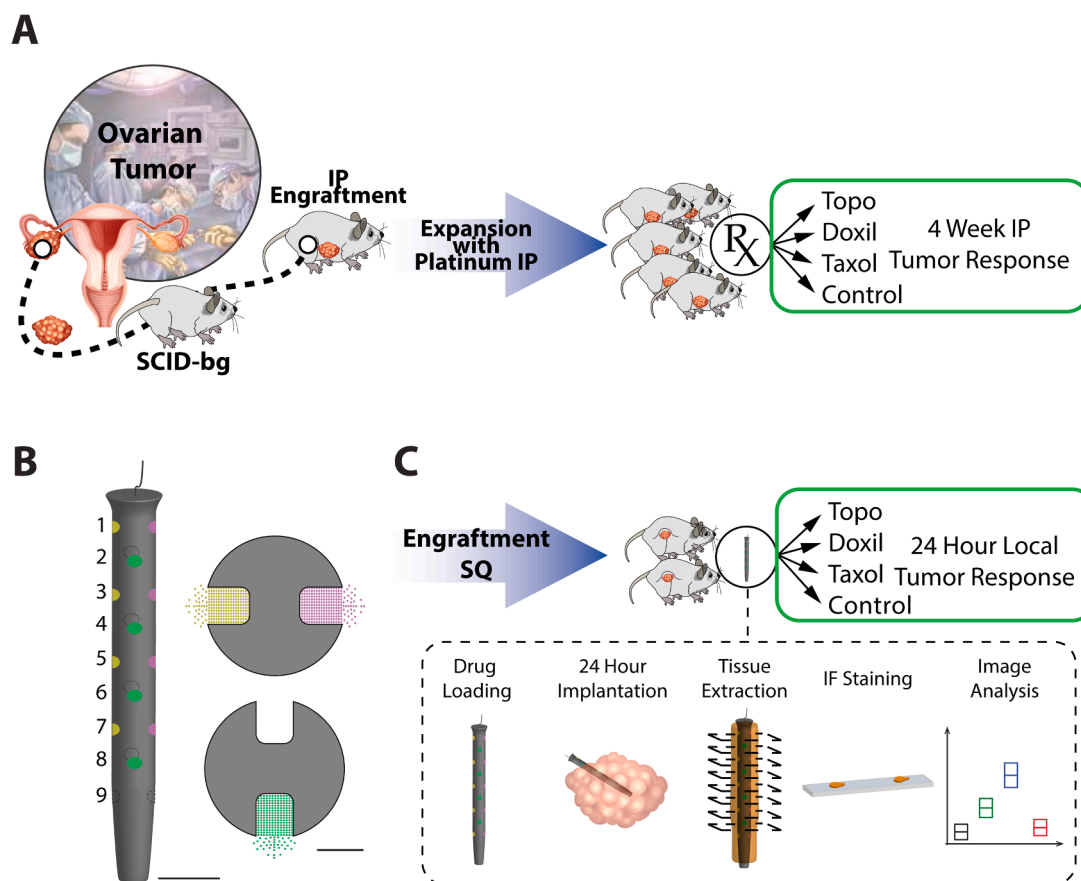


Fig. 1. Schematic of *in situ* drug sensitivity assay. (A) Ovarian tumor tissue is harvested during debulking surgery and engrafted IP in immunodeficient mice. The tissue is then expanded with platinum pretreatment followed by regrowth and 4 weeks of IP drug treatment. Tumor size is tracked with peritoneal ultrasound. (B) The microdevice is filled with up to 3 compounds in quadruplicate leaving 6 no-drug control wells. Drug is released from each well in distinct locations with minimal crosstalk. Wells are arranged in 9 levels each containing 2 wells. Scale bars 1 mm (left) and 0.25 mm (right). (C) Banked tissue is engrafted SQ in immunodeficient mice, and a drug-loaded device is implanted for 24 h. The device is extracted with surrounding tissue, the tissue is stained for drug response via immunofluorescence, and drug response is quantified with digital image analysis, which can be used to predict IP treatment outcomes.

area percent relative to the starting baseline size (representative ultrasound seen in Fig. S1). Control mice served as a reference for growth kinetics but sensitivity to treatment was defined as regression below baseline. Animal survival was based on “time to event”, with the event being moribund criteria as defined by IACUC guidelines. Briefly, all animals were sacrificed if any of the following were met: weight loss >20%, inability to ambulate or access food/water, tumor ulceration, estimated tumor size >10% of bodyweight, or low body conditioning and/or behavioral score. Animal death was not the endpoint. For each PDX model, repeated measures analysis of variance implemented via linear mixed effects models were used to compare growth trajectories between drugs [39–41] (Supplemental Methods).

Device fabrication and preparation

Implantable microdevices, adapted from Jonas et al. [33], were used to assess the local subcutaneous (SQ) ovarian PDX tumor response to short-term exposure to the same second-line chemotherapies used IP. Devices were implanted SQ rather than IP because of greater consistency of implantation compared with smaller IP tumors, the long-term goal of shortening the time for PDX engraftment, and prior experience with implanting into SQ tumors [32,33,35]. Cylindrical microdevices with 750 μm (diameter) \times 6,173 μm (length) were manufactured using standard micromachining as previously described (Figs. 1B, S2). Devices were made of medical-grade Delrin acetal resin. This material was chosen due to its biocompatibility, structural rigidity and machinability. Devices contained 18 wells, each with a diameter of $201 \pm 5 \mu\text{m}$ and

depth $250 \pm 5 \mu\text{m}$. The wells were divided in four columns, with two columns of 4 wells, and two columns of 5 wells (Fig. S2). Manufacturing of devices was outsourced to Treat Manufacturing (Sonora, CA, USA). 0.008-gauge nitinol wire (Malin Co, Brookpark, OH, USA) was placed at the top of the device to aid in device retrieval and tissue processing (Supplemental Methods). Multiple quality controls were integrated into the process to ensure consistent, reliable dosing of drugs into the tumor microenvironment.

Drug formulation

Drugs placed in the microdevices were formulated in a biocompatible polymer matrix (polyethylene glycol, PEG) to ensure minimal crosstalk between wells and matched intratumoral drug concentration achieved by systemic administration as outlined previously (Supplemental Methods) [33]. Non-liposomal doxorubicin was used with the devices, as intratumoral delivery negates the need for the pharmacokinetic advantages afforded by liposomal encapsulation that are required with clinical administration. Drug was manually loaded into each micro-well using stainless steel microtools. Each device contained up to 6 empty control wells and 12 drug-filled wells (4 wells for each of 3 drugs).

SQ tumor engraftment and device implantation

Severe combined immunodeficient (SCID) beige mice were injected subcutaneously with processed viable frozen ovarian tumor in a biosafety cabinet using sterile technique. Viable frozen stock was

thawed and processed to remove freezing media then loaded into dispensing syringes equipped with 16g x 1/2 inch needles. 0.1–0.2 cc of minced tumor was prepared in a 1:1 ratio with McCoy's 5A Modified Medium (MT-10-050-CV, Corning Life Science, Tewksbury, MA, USA). Mice were anesthetized using inhalation of metered isoflurane with oxygen during tumor injection. Tumor size was tracked weekly with calipers, and volumes were calculated with the formula $4/3\pi \times r_1^2 \times r_2$ ($r_1 < r_2$), in which r_1 is the smaller radius.

Once tumors reached 1 cm³, a microdevice was implanted. A small skin incision (<5mm) was made and a 19-gauge biopsy needle was inserted into the tumor. The device was inserted into the open end of the needle and gently pushed into the tumor with the help of an obturator. The needle was then retracted, and the small incision wound closed with tissue glue (3M Animal Care Products, St. Paul, MN, USA). All animal protocols were approved by both the Committee for Animal Care of the Massachusetts Institute of Technology and the Institutional Animal Care and Use Committee of the Mayo Clinic. A total of ten mice across seven PDX lineages were used. Each mouse had one device with each treatment condition in at least triplicate (For each drug, $n = 3/\text{animal}$). Differences in sample numbers were due to tissue damage during histology processing.

Tissue processing

Twenty-four hours after device implantation, animals were euthanized using CO₂ asphyxiation and tumors explanted with the device intact. This time was chosen based upon the dissolution time of the drug-polymer matrix and to minimize foreign body response obscuring tumor response. Tumors were processed with the assistance of the Koch Institute Histology Core (Supplemental Methods). Briefly, devices and surrounding tissue were exposed via manual extraction, and paraffin processed via a custom embedding block (Fig. S4). Tissue and device were sliced at each level of drug release (9 levels, 18 sites of release), and the tissue was stained with hematoxylin and eosin (H&E) and via immunofluorescence (IF) (Fig. S4). IF staining was done to identify all cells (DAPI), apoptotic activity (cleaved caspase-3, CC3), proliferation (Ki67), and malignant cells (pan-cytokeratin, PanCK or Human Lamin A/C). All slides were digitally scanned. Tumor marking stains were used to distinguish murine stroma (only DAPI positive) from human carcinoma (PanCK positive). Human Lamin A/C staining was also used as a tumor marker to more simply distinguish murine stroma and human carcinoma, but PanCK was the preferred method as it is a clinical standard stain and can be used in patient tumors.

Image analysis

Immunofluorescent images (captured via Aperio ImageScope (Leica Biosystems, Buffalo Grove, IL, USA)) were quantitatively analyzed via a custom MATLAB (MathWorks, Natick, MA, USA) script with each fluorescent channel independently loaded. Background was removed from analysis. Channels were binarized based upon a user-defined threshold. CC3, Ki67, and PanCK thresholds were set based upon the mean of the Gaussian fit of intensities, and thresholds for Lamin and DAPI were set to one standard deviation less than the mean (Fig. S7). A blurring factor was added to account for differences between pixel size and cell size/location.

Standardized trapezoidal regions of interest (ROIs) were placed in correspondence to areas of drug release and tissue background (Fig. S7). Device layouts were predetermined before implantation, and post-implantation positions were determined in reference to doxorubicin visualized by fluorescent imaging of unstained tissue (Fig. S8). Measurements of apoptosis index (AI) and proliferation index (PI) were calculated based upon Eqs. 1-4, representing changes in apoptosis or proliferation in regions of drug treatment compared to background regions away from sites of drug release. AI and PI measurements were confined to carcinoma by colocalizing CC3 or Ki67 signals with a tumor

marking signal (PanCK or Lamin A/C). Stroma was measured as the percentage of cells in a given region not positive for a tumor marking stain. Measurements were done using both PanCK and Lamin as tumor markers. Measurements taken from ROIs were excluded based upon preset rules (Supplemental Methods).

$$AI_{Carcinoma} = \left[\frac{PanCK^+ CC3^+}{PanCK^+} \right]_{ROI} - \left[\frac{PanCK^+ CC3^+}{PanCK^+} \right]_{Background} \quad (1)$$

$$AI_{AllCells} = \left[\frac{DAPI^+ CC3^+}{DAPI^+} \right]_{ROI} - \left[\frac{DAPI^+ CC3^+}{DAPI^+} \right]_{Background} \quad (2)$$

$$PI_{Carcinoma} = \left[\frac{PanCK^+ Ki67^+}{PanCK^+} \right]_{ROI} - \left[\frac{PanCK^+ Ki67^+}{PanCK^+} \right]_{Background} \quad (3)$$

$$PI_{AllCells} = \left[\frac{DAPI^+ Ki67^+}{DAPI^+} \right]_{ROI} - \left[\frac{DAPI^+ Ki67^+}{DAPI^+} \right]_{Background} \quad (4)$$

Statistical significance was determined via a single-tailed student's T-test with unequal variance assumed. Tukey's honest significant difference (HSD) was used to compare drug and control for input features for the prediction classifier.

Classifier development

A forward-backward stepwise feature selection machine learning classifier (Scikit-Learn Python tool kit) based upon linear regression was developed to predict IP treatment outcomes of all three drugs in ovarian IP PDX tumors using the results of *in situ* drug sensitivity screening in SQ ovarian PDX tumors [42]. IP treatment outcomes were treated as a binary 'ground truth' based upon quantitative estimates of change from baseline calculated via the mixed effects model mean estimate at Day 28 minus Day 0 (Table S1, Supplemental Methods). Importantly, regression of tumor below baseline better represents a desired clinical outcome of partial or complete response to therapy. Thus, tumor regression (slope < 0) was chosen as a more conservative estimate of drug sensitivity compared to the alternative endpoint of tumor growth inhibition (slope statistically significantly less than control). Statistical comparisons of SQ PDX tumor response to local drug exposure (AI and PI) and stroma content between areas of drug release and control wells within a single tumor were used as inputs to the classifier as well as measurements patient tumor characteristics (Table 2). Tukey's Honest Significant Difference (HSD) tests were used for comparisons, resulting in 3 statistical outputs per comparison, leading to a total of 23 possible features. Feature selection was driven by area under the curve (AUC) optimization.

Five-fold cross-validation was used by generating 5 replicate datasets with different training and testing set partitions to provide adequate validation with a small sample size [43–45]. Each row of data represents comparisons of measurements of drug sensitivity between control and one drug in a single animal. Leave one out cross-validation was also used by leaving out data from a single PDX. Classifiers were also generated using multiple measurements of ground truth including *p*-value thresholds from the mixed model analyses of IP treatment response ($p = 0.05, 0.01, \text{ and } 0.001$) as well as a projected mean tumor size relative to baseline being less than 1 at day 28 of the IP study. These methods were completed using both lamin A/C and PanCK as tumor markers.

The best performing classifier was used to predict the efficacy of MK-1775 using data from devices containing MK-1775 in a pilot study (Fig. S26, Table S2). Predictions for efficacy in PH354 were validated with results from IP studies. Sensitivity in other PDX lineages were not validated IP.

Table 2
Feature set.

	Location	Cells	Features Difference of means	Tukey HSD <i>q</i> statistic	Null hypothesis rejection*	IF Percent cells stained
AI	PDX	All	X	X	X	
	PDX	Carcinoma	X	X	X	
	PDX	Stroma	X	X	X	
PI	PDX	All	X	X	X	
	PDX	Carcinoma	X	X	X	
Stroma	PDX		X	X	X	
	Patient					X
CC3 expression	Patient	All				X
	Patient	Carcinoma				X
Ki67 expression	Patient	All				X
	Patient	Carcinoma				X

Results of *in situ* drug sensitivity testing in SQ ovarian PDX tumors and patient tumor characteristics were used as input features in a machine learning classifier to predict tumor response in IP treated animals. *Rejection levels of 0.1, 0.05, 0.01 considered.

Results

Immunofluorescence staining and image analysis

Histological techniques have been previously used to understand the phenotypic response of tumor to local drug exposure after microdevice implantation [32–38]. Hematoxylin and eosin (H&E) staining was used to characterize tissue morphology (Fig. 2A, B). A non-uniform mix of epithelial carcinoma and tumor-associated stroma was observed throughout the tumors (Figs. 2A, S5). Immunofluorescence (IF) techniques were used so that multiple tissue markers could be assessed in parallel. IF provided the additional advantage of enabling high-throughput digital image analysis that can distinguish between human epithelial carcinoma and murine stroma (Figs. 2C, D, S5). Tumor response was assessed via staining for apoptosis (cleaved caspase-3, CC3) and proliferation (Ki67) (Fig. 2C, D). Human epithelial carcinoma was distinguished from murine stroma in PDX tumors using pan-cytokeratin (PanCK) and nuclear (DAPI) staining (Fig. 2C, D). PanCK is a clinically validated marker used to define epithelial cancer and was included to allow the tissue analysis platform to work within existing clinical workflows. Human lamin A/C staining was also used to distinguish between human epithelial carcinoma and murine stroma (Fig. S6).

IF stained tissue was quantitatively analyzed using a custom image analysis program. Regions of interest (ROIs) of standardized shape and size were then drawn to identify the two sites of drug release at each level and tissue background, using fluorescent images of doxorubicin autofluorescence and tissue tags to denote device layout (Figs. 2E, S7, 8). Stroma was identified as DAPI-positive pixels not positive for a tumor marker (PanCK or lamin A/C) (Fig. 2F). Apoptosis and proliferation were defined by the apoptotic index (AI) and proliferation index (PI) respectively (Eqs. 1–4) based upon previous work [32]. AI and PI were calculated as values above the background levels of proliferation and apoptosis to account for inherent apoptosis and proliferation in each tumor. Background regions were defined as areas of tumor away from sites of drug release and control wells that do not overlap with ROIs selected as sites of drug release (Figs. 2E blue, S7). Apoptosis and proliferation measurements were localized to carcinoma cells by colocalizing CC3 or Ki67 signals with PanCK (Fig. 2G, H, Eqs. (1), (4)). The same measurement was done using lamin A/C in place of PanCK (Fig. S6). Apoptosis measurements were also localized to stromal cells by colocalizing CC3 or Ki67 to stroma pixels (DAPI without PanCK or lamin A/C). AI and PI measurements using PanCK or lamin as a tumor marker were correlated across tissue samples (Fig. S9). Similar analyses were done with a single tissue sample from each patient's original tumor, and baseline tumor characteristics were compared to corresponding PDX tissue (Figs. S10, S11). Further, histology images for other PDXs can be seen throughout the supplement.

Quantifying tumor response and accounting for variations in stroma content

Stromal content was quantified at each level of the device using PanCK as a tumor marker, both near sites of drug release and distal from the device in tissue background. High degrees of variation in stromal content were seen within a single tumor among mice of the same PDX lineage, controlling for passage number, (25–75%, Fig. 3A), and among mice with different PDX lineage tumors (10–75%, Figs. 3B, S12). Measures of apoptosis and proliferation were made with and without accounting for these variations by colocalizing CC3 or Ki67 with PanCK (Figs. S13, S14; Eqs. (1), (3)). Apoptosis was also localized to stromal cells only (Fig. S13). Standard deviation was reduced 2.6-fold in AI measurements taken at control microwells when AI was confined to carcinoma cells (Fig. 3C, D). Topotecan was found to induce significantly higher apoptosis compared to control when the measurement was confined to carcinoma only, but this increase in AI was not significant when the measurement was taken in all cells. Similar results were seen using lamin A/C staining to limit measurements to carcinoma cells (Figs. S15, S16).

Systemic drug sensitivity was quantified in 206 animals with IP PDX tumors treated systemically via IP injection (Figs. 4A–G, S17). Each cohort was comprised of at least 3 mice (Fig. S18), with differences in cohort size due to differences in PDX engraftment rates and expansion time. Animal dropout due to animal death or tumor size exceeding euthanasia criteria varied across PDXs and treatment cohorts due to variability in inherent tumor growth rates and drug toxicity (Fig. S17). IP tumor size during systemic drug administration was analyzed via mixed effects models to account for correlation between repeated measurements (Figs. S17, S18) [39–41]. A summary of the models and statistics can be found in Table S1.

Microdose drug sensitivity was measured in 10 animals with SQ tumors of 7 PDX lineages implanted with a drug-loaded microdevice (Fig. 4H–U). Each drug was tested in at least triplicate within a single microdevice implanted in an animal. Measurements of AI and PI localized to carcinoma across mice of the same PDX can be seen in Fig. 4H–U. Data from all SQ tumor studies can be seen individually in Figs. S13–16.

Predicting treatment outcomes using forward-backward feature selection

A forward-backward feature selection classifier was developed to predict IP PDX treatment outcomes using short-term phenotypic response of SQ PDX tumors to locally-delivered therapy. Measurements of phenotypic response in treated regions compared to control and baseline tumor characteristics were used as inputs (Table 2). A 4-feature (AI in stroma, two measurements of PI in carcinoma, baseline patient tumor Ki67) classifier was identified that predicted IP tumor response to any one of the three drugs from SQ drug sensitivity screening with a cross-validation AUC of 1.00 and an accuracy of 95.2% and AUC of 1.00

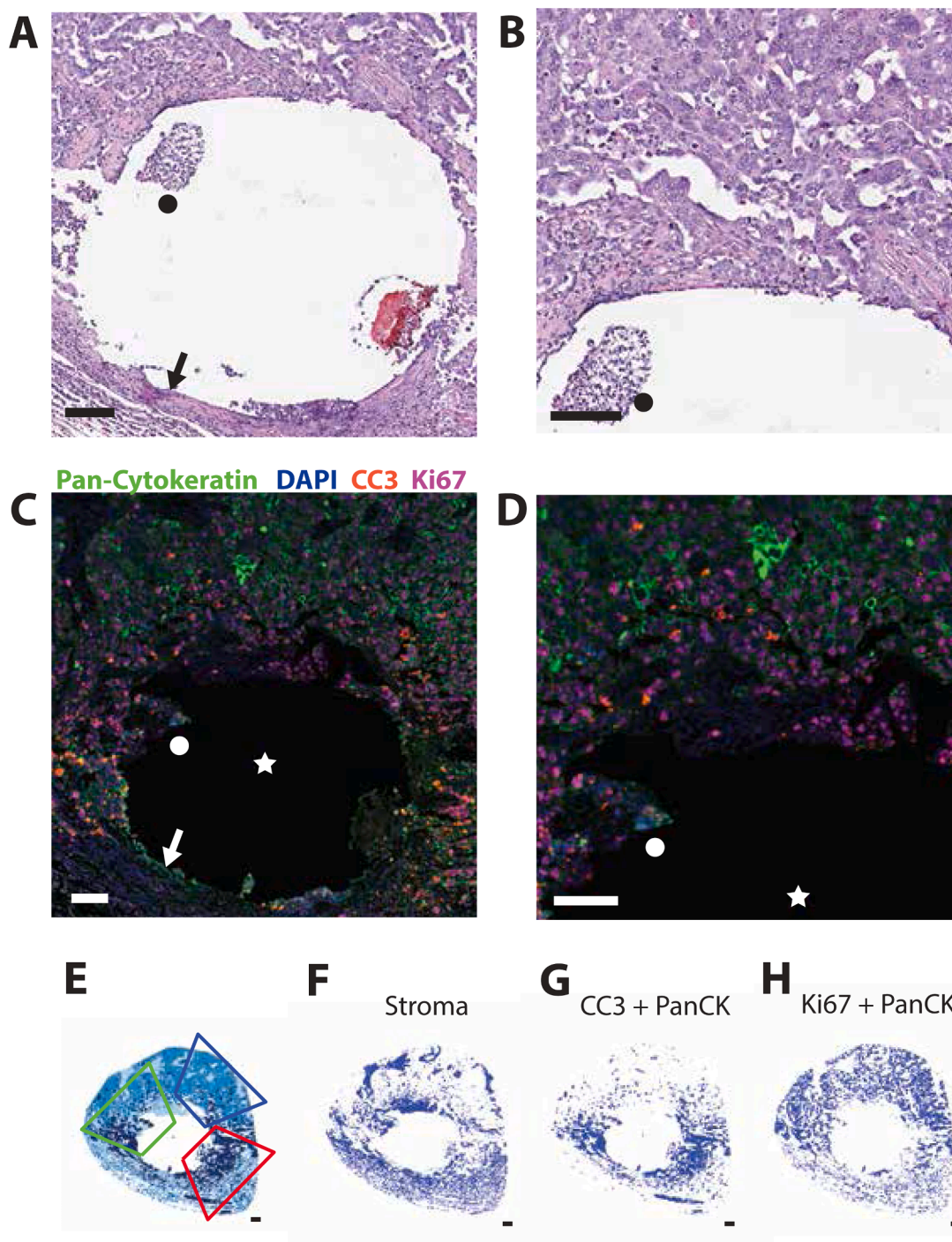


Fig. 2. Immunofluorescence staining quantifies drug response and stroma. (A) Hematoxylin and eosin stained tissue around device and (B) at site of drug release. (C) Immunofluorescence stained tissue around device and (D) at site of drug release. Tumor is stained with pan-cytokeratin (green). Stroma is identified by DAPI (blue) without a pan-cytokeratin. Apoptosis is identified by CC3 (red), and proliferation is identified by Ki67 (purple). (E) Drug response is quantified in regions of interest: at sites of drug release (green and red) compared to background (blue). (F) Stroma is identified by DAPI positivity and a lack of pan-cytokeratin. (G) Apoptosis is localized to carcinoma tissue by pan-cytokeratin and CC3 positivity. (H) Proliferation is localized to carcinoma tissue by pan-cytokeratin and Ki67 positivity. Arrow indicates stroma. Stars indicate microdevice location. Dots indicate tissue tag. Scale bars 100 μ m. Tissue from PH723 animal A.

when validated on testing data sets (Fig. 5A, B). The prediction model was cross-validated using 5-fold cross-validation to account for a small dataset size by replicating the data into 5 sets each with a different 20% reserved for validation [43–45]. The first features that maximize AUC are listed in Table 3.

When thresholds that optimized sensitivity and specificity were used, predictions had an overall sensitivity of 100% and specificity of 92%,

with 1 false positive prediction made for doxorubicin out of 20 total predictions (Table S2). Similar results were observed for classifiers trained with data using filters to exclude regions of high stroma and for classifiers trained to predict ground truth based upon growth inhibition rather than tumor shrinkage (Figs. S19, S20).

Seven additional classifiers were generated with leave one PDX model out cross-validation (1 for each PDX left out). Comparison of

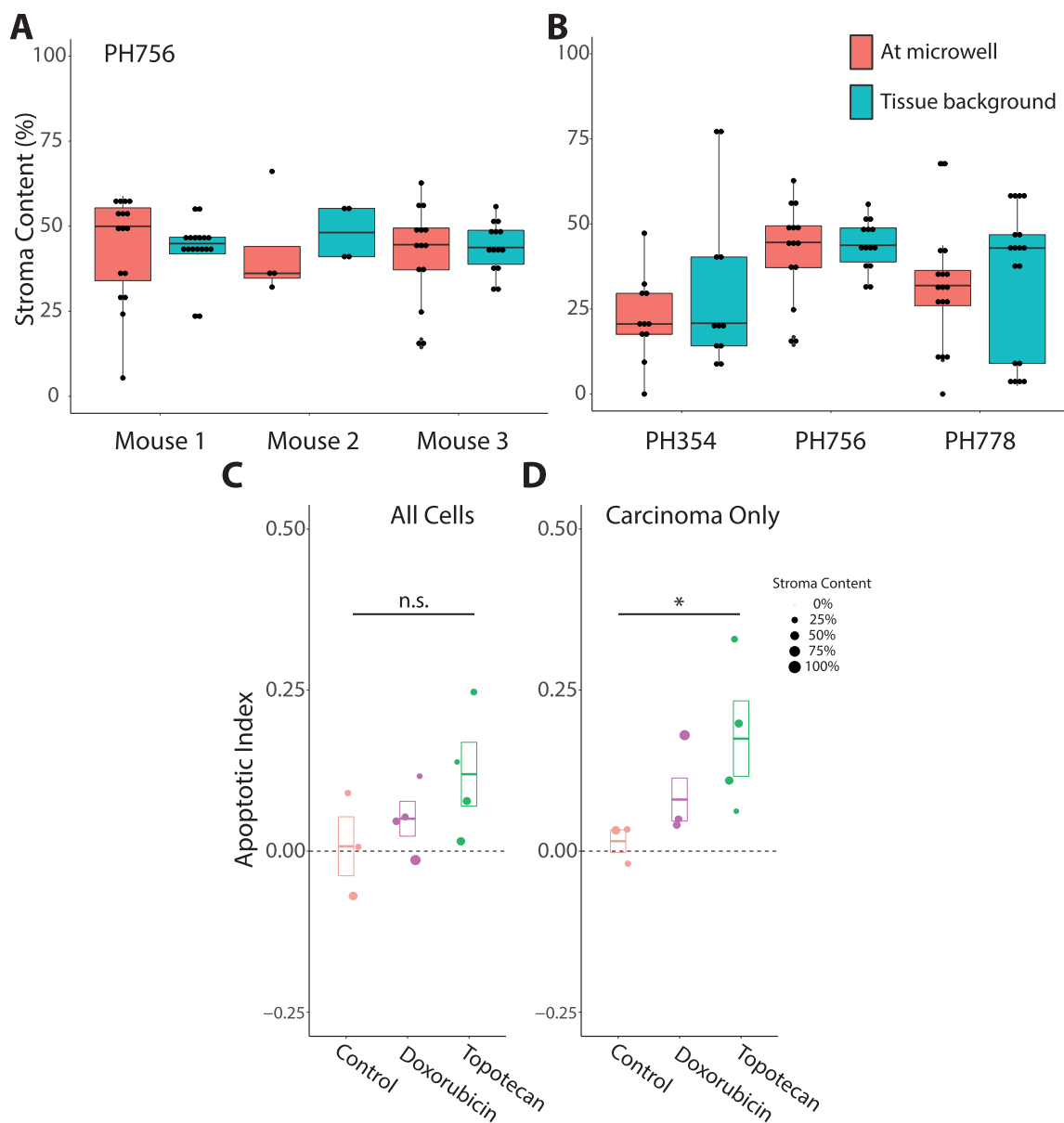


Fig. 3. Stroma varies within PDX tumors and must be accounted for in drug response analyses. (A) Stroma content within tumors varies between sites of drug release (red) and in drug-naive areas (teal) and among tumors of the same PDX. (B) Further variation is seen among tumors of different PDX origin. Box and whisker represent median, 25%, and 75% quantiles. Each point represents a single measurement within a mouse. (C) Representative chart showing apoptotic index in all cells resulting from drug exposure compared to control in a single animal. (D) Localizing apoptosis measurements to carcinoma only reduces variability in control measurements and results in statistical significance. Box represents mean \pm standard error. Dot size represents stroma content at the site of the measurement. * $p < 0.05$, student's t-test, single tail, unmatched. Example AI data from PH626 animal A.

these models tested if a single PDX was driving predictions. The results of the predictions were not dependent on the presence of a single PDX in the training set (Fig. 5C). The average maximum AUC achieved by these 7 classifiers was 0.91. The top four features for each classifier were consistent across leave one out datasets, including multiple measurements of apoptosis and proliferation (Table 3). Similar results were seen using lamin A/C staining (Fig. S21).

Extending predictions to a novel drug class

Although the classifiers were developed to predict IP chemotherapy response rather than response to small molecule inhibitors, efficient assessment of novel targeted therapies using an *in situ* drug response assay could provide a valuable tool for preclinical drug development and stratifying patients for clinical trials. To explore this possibility, a pilot

study was done using all 8 classifiers (7 leave one out, 1 with all PDXs) to predict sensitivity to adavosertib (a Wee1 inhibitor currently under clinical investigation in ovarian cancer, adavosertib) based upon the same phenotypic response analysis completed to assess cytotoxic chemotherapy sensitivity. A device containing adavosertib was implanted into SQ PDX tumors from PH354, a high grade serous tumor, which is of the subtype that has seen clinical response to adavosertib. Tumor response to adavosertib was assessed using the methods above (Fig. 5D) and results were used to predict systemic efficacy using the eight classifiers trained on response to cytotoxic therapy. All eight classifiers predicted IP adavosertib sensitivity in PH354, including the classifier not trained with data from PH354 (Fig. 5E). The efficacy of adavosertib was validated in PH354 by systemic treatment of IP PDX tumors, resulting in an immediate and progressive regression to an average of less than 50% of original tumor size compared to a 3-fold

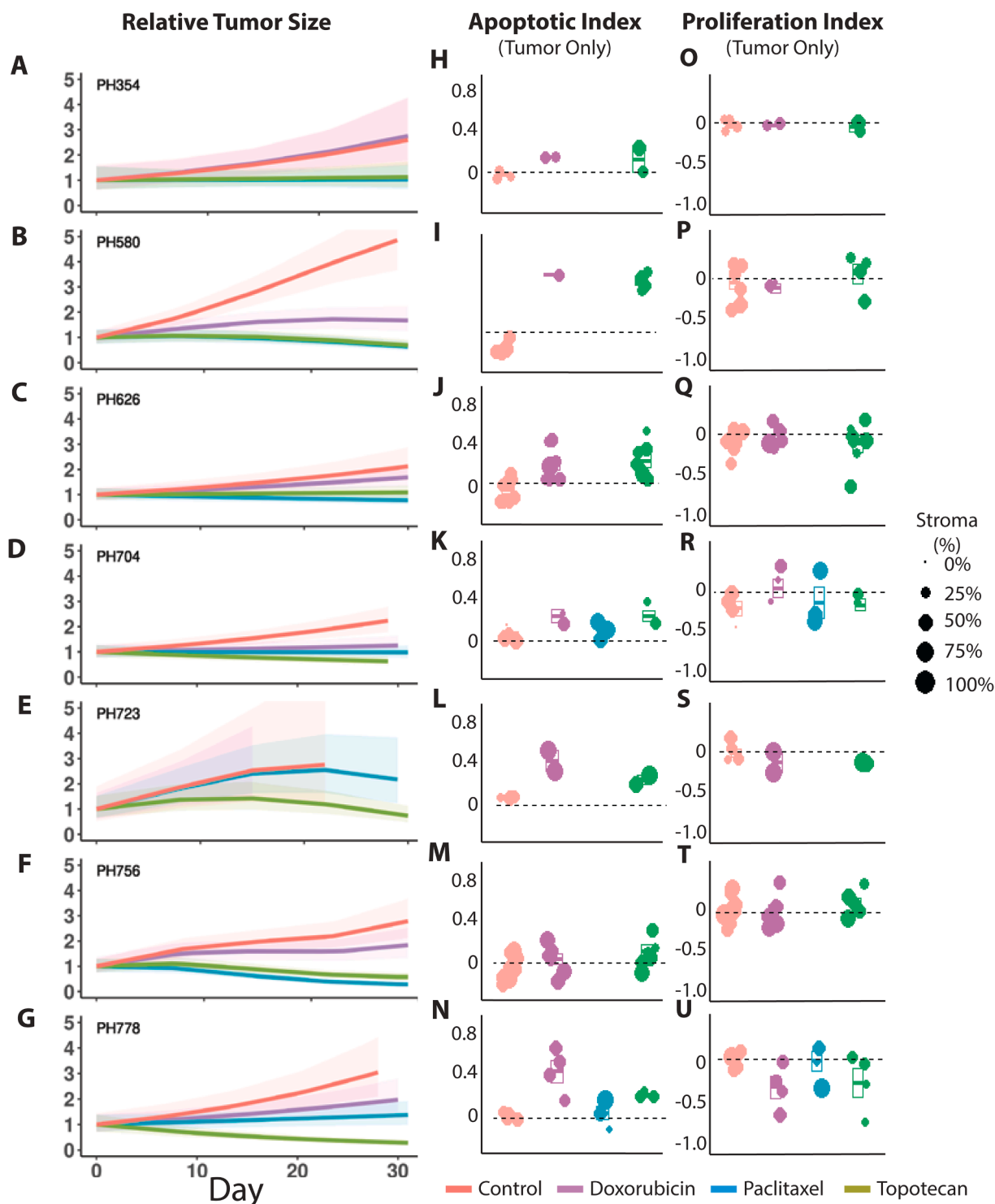


Fig. 4. Systemic and local sensitivity to chemotherapy across 7 ovarian PDX tumors. (A–G) Relative tumor size measured by ultrasound during 4 weeks of weekly IP treatment studies. Paclitaxel 33 mg/kg, Doxorubicin-PEG 2.4 mg/kg, Topotecan 10 mg/kg. Linear and quadratic mixed effect models are used for estimation of growth curves and hypothesis testing accounting for correlation between repeated measurements. Mean \pm 95% confidence interval. (H–N) Apoptotic index and (O–U) proliferation index localized to epithelial carcinoma only after local drug exposure across 7 PDXs, each with up to 2 mice. Box represents mean \pm standard error. Dot size represents stroma content at site of drug release.

increase in tumor size in control animals over 28 days (Figs. 5F, S17, 18).

Discussion

We have shown how microdevices acutely implanted in SQ ovarian PDX tumor models can predict overall IP ovarian PDX tumor response to

various IP-delivered drugs with an average AUC of 0.91 using only 3, 4 measurements per drug in each PDX tumor. This represents a significant step forward in making personalized PDX drug sensitivity screening clinically practical and provides preliminary evidence for the investigation of *in situ* drug sensitivity screening in patients’ tumors directly. Multiplexed IF imaging of explanted tumor tissue surrounding the

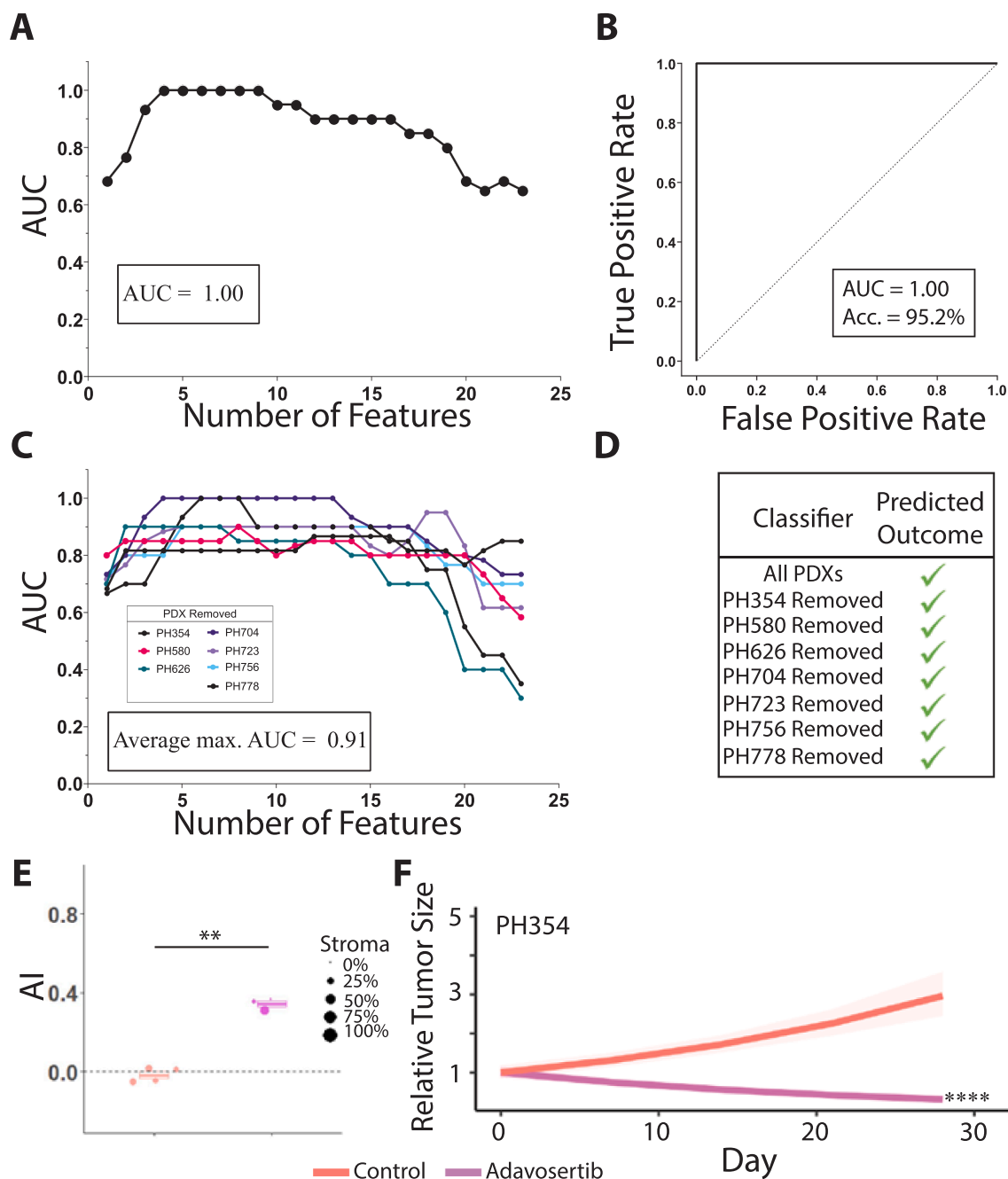


Fig. 5. Classifier predicts treatment outcomes. (A) Forward-backward feature selection classifier optimized for area under the curve (AUC) using data from all PDXs representing a 4 feature classifier with AUC of 1.0. (B) Receiver operator characteristic (ROC) curve using 4 feature classifier represents AUC of 1.0 and accuracy of 95.2%. (C) Forward-backward feature selection classifiers using data with one PDX removed optimized for AUC. (D) Predictions of ADAVOSERTIB efficacy in PH354 using multiple classifiers. (E) Apoptotic index localized to carcinoma after local ADAVOSERTIB exposure in PH354. Box represents mean \pm standard error, dot size corresponds to stroma at site of drug release. (F) Relative tumor size measure via ultrasound during 4 weeks of weekly IP ADAVOSERTIB treatment in PH354. Linear mixed effect model estimates growth curves for hypothesis testing accounting for correlation between repeated measurements. ** $p < 0.01$, student's t-test, single tail, unmatched. **** $p < 0.0001$ Wald F-test.

microdevices enabled a classifier to accurately predict overall tumor response to systemic IP therapies based upon local phenotypic drug response and baseline tumor characteristics. No significant difference was observed when classifiers were trained with leave one PDX out cross-validation and AUC was not significantly decreased (AUC = 1 using all PDXs and an average of 0.91 in leave one out cross-validation). Thus, the classifier was not overly reliant on a single PDX. The classifier was also developed using the most conservative estimate of ground truth, tumor regression rather than tumor growth suppression relative to

control. The use of tumor regression as an endpoint is representative of a desired clinical outcome of partial and complete responses to therapy. These predictions were made with significantly fewer animals per PDX (1-2 SQ vs. 20+ IP) due to parallel drug microdosing, which enables PDXs to be a more cost-effective tool for personalizing therapy than the current standard. Standard staining was also used, which would allow for more straightforward implementation of the platform into standard clinical pathology workflows and measurements are drug mechanism agnostic.

Table 3
Identified feature sets.

Data Set	AI			PI		Stroma	Patient Tissue	
	All Cells	Carcinoma	Stroma	All Cells	Carcinoma		CC3%	Ki67%
All PDXs (AUC = 1.0)			N		M, Q			All Cells
PH354 Removed (AUC = 0.87)	M, Q, N	M						
PH580 Removed (AUC = 0.90)	N	M, N	M					
PH626 Removed (AUC = 0.90)		Q	N					
PH704 Removed (AUC = 1.0)			N	Q	Q			Carcinoma
PH723 Removed (AUC = 0.95)		M, N, Q	M					
PH756 Removed (AUC = 0.90)	M		M	Q		N		
PH778 Removed (AUC = 1.0)	M	M	N	N				

Significant features identified as predictive of IP drug response as determined by classifier generation. Top four features are listed for classifiers generated with data missing one PDX or top features before AUC plateaus. M: difference of means, Q: Q score, N: null hypothesis rejection.

Our study revealed the extent of heterogeneity of PDX tumors. Histological sections at various points of a PDX tumor had drastically different architecture with stromal content ranging from 0 to 100% among multiple regions of the same tumor (Fig. S12). This highlights the importance of experimental replicates in drug microdosing from a single device as well as measurements of tumor response to drug that account for this heterogeneity. Here we used at least three experimental replicates per treatment group. The inclusion of PanCK as a tumor marker allows for such measurements to take place without changing clinical histology workflows. We also wanted to investigate the potential impact of stroma in treatment response to each drug (Figs. S22–S25). We saw preliminary evidence that high stroma correlates with less apoptosis for some drugs (topotecan) (Figs. S22, 23), and stromal apoptosis contributes substantively to predictive classifiers of overall tumor response (Table 3). This warrants further investigation to specifically examine the role of stroma and the tumor microenvironment in drug sensitivity and the potential for combining cytotoxic and anti-stromal drugs in ovarian cancer. In contrast, we did not see significant trends between changes in proliferation after cytotoxic chemotherapy and the amount of stroma (Figs. S24, 25).

Across the drugs and models, we found both apoptosis and proliferation to be important in predicting treatment efficacy across the drugs and PDX models (Table 3) despite previous studies relying upon apoptosis alone. The 4-feature classifier generated using data from all PDXs identified apoptosis in stromal cells and inhibition of proliferation to be significant in predicting longer term outcomes. While twenty four hours is relatively short for apoptosis of carcinoma cells to occur [46], we hypothesize that stromal apoptosis and a reduction in proliferation of carcinoma cells may be leading indicators for eventual tumor regression. Time points longer than 24 h may be beneficial to allow enough time for apoptosis to occur in response to certain drug classes or in relatively lower metabolically active tumors; however, this must be balanced with the emergence of a significant foreign body response obscuring measurements of drug response and the time course of CC3 expression and apoptosis. Patients' baseline tumor proliferation was also found to be significant, which suggests predicting treatment outcomes must also include characteristics of treatment-naïve tumor (second-line treatment naïve in the case of platinum resistant/refractory tumors or PARPi naïve in the case of predicting maintenance therapy sensitivity). The inclusion of both apoptosis and proliferation in addition to other measurements of tumor morphology and patient tumor characteristics allows the platform to be adapted to screen a wide range of drug classes, even those that may not induce apoptosis quickly or differentiate drugs that elicit apoptosis without gross tumor shrinkage.

We also found preliminary success in predicting the sensitivity of a

single PDX to a small molecule inhibitor not included in the training data set as a pilot use case of identifying patients for experimental treatment. This represents success in the most conservative use case: a novel therapeutic in a novel tumor. This supports ongoing research into adavosertib as a potential clinically efficacious drug for ovarian cancer. The successful prediction of adavosertib sensitivity also demonstrates the potential promise of this platform in preclinical drug development. The combined experimental and computational approach enables increased throughput and parallel evaluation of new compounds or combinations *in vivo* without the need for large animal cohorts (10 with device vs. 206 systemic). Multiple concentrations of a single agent can also be tested in parallel. Single cell lines or PDXs can be used during drug development to screen multiple compounds and generate predictions of tumor response that can be validated with systemic studies. Novel drug classes (novel mechanism of action or molecule type) can be evaluated without the need to optimize drug distribution within the tumor. No secondary encapsulation is required to improve distribution after systemic administration for preliminary testing, for example, as seen with the use of doxorubicin in the device versus liposomal doxorubicin used IP and clinically. This would provide efficient and cost-effective insights on mechanism of action and allow for accelerated drug development.

There exist a number of limitations to this approach and potential for future applications. Data was analyzed from only 7 patient-specific PDXs, precluding comparisons between drug sensitivity and clinical treatment outcomes. Other classifier development work generally requires larger sample sizes, but 7 distinct PDX lines is a relatively large study. Further work is required to fully develop a robust classifier system for treatment prediction. This work utilized ovarian tumors exclusively and may have to be adapted for use in other cancer types. The 24 h time point to assess tumor response to a single microdose of drug is based on the dissolution time of the polymer-drug formulation used. Future work could compare this with tumor response assayed at longer or shorter time points. Appropriate loading of various drugs in a single well could enable sequential dosing of different therapies. Future work could also utilize this platform to screen sensitivity of tumors to other therapy classes (gene therapies, radiotherapy) without significantly changing the processing pipeline. Our observations show that the response of a micro-region of PDX tumors, despite tumor heterogeneity, is predictive of the overall tumor response when the heterogeneity is considered. An outstanding question is how small a region of tumor can be targeted or how many regions of tumor tissue must be targeted while still reflecting overall tumor behavior and sensitivity. This could potentially allow for even smaller devices and greater multiplexing of drugs to be screened. Future studies may also explore the inclusion of more features that may affect tumor response to therapy (i.e. patient demographics, oncogene/

suppressor gene status) to optimize prediction accuracy. Only a limited amount of patient demographics were available from the tumor repository for this study.

Current clinical studies of the microdevice platform can be improved by the inclusion of the high-throughput image analysis and ML-driven computational toolkit outlined here. This approach can enhance the applicability of the platform and allows for continual improvement in accuracy through further classifier development. The next step for this technology includes a clinical validation study in ovarian SQ PDX tumors with an expanded cohort of patients. Clinical implementation of the platform in ovarian cancer patients would require an additional procedure before debulking surgery for device implantation. We thus believe near-term studies must validate the platform using PDXs first. Direct SQ PDX engraftment in other cancer types has been shown to generate tumors more quickly than orthotopic engraftment (less than 3 months) due to the increase vascularity of the SQ space and the ability to engraft large tumor volumes [22–25,47–49]. This approach would also not require tissue expansion, further saving time and animals. Direct SQ PDX engraftment followed by *in situ* drug screening could provide predictions of second-line therapy efficacy for patients with platinum-refractory tumors (growth during platinum therapy) in a clinically relevant time frame (less than six months). PDXs derived from patients with platinum refractory tissue have inherent platinum resistance, thus drug screening would take place in tissue representative of the tissue exposed to systemic second-line therapy. PDXs may also be used to predict sensitivity to PARPi for patients with platinum sensitive *BRCA1/2* wildtype tumors. There are currently no functional assays for predicting PARPi sensitivity for these patients. Homologous recombination deficiency (HRD) score testing, while practice-changing for clinicians, does not provide a functional prediction of PARPi response, only a relative history of genomic instability. PDXs, derived from patients during debulking surgery, implanted with devices loaded with PARPi therapy using the method described here may also be used to screen patients without the need for additional procedures (device implantation/retrieval). This implant platform can also be adapted for direct implantation in patients' tumors after recurrence or before PARPi therapy followed by biopsy using image-guided implantation/retrieval device as a tool to be combined with HRD scoring for selecting patients for PARPi maintenance [36]. A combined experimental and computational approach using either the direct implantation of the device into patients' tumors or the generation of SQ PDXs with device implantations could further inform personalized therapy choices for patients by providing predictions of treatment efficacy in a matter of days to weeks. These approaches avoid the time and expense required to conduct traditional IP PDX studies, instead examining the sensitivity of a patient's tumor through multiplexed microdosing.

We have demonstrated that a 24 h assay in SQ ovarian PDX tumors using a drug-loaded implant and ML classifier can be used to predict long-term treatment outcomes for IP ovarian PDX tumors in a clinically relevant time frame. IP ovarian PDX tumors have been shown to be predictive of patient outcomes, thus the 24 h *in situ* sensitivity screening assay may be predictive of patient outcomes directly. The device may also be directly implanted into patients' tumors to allow for personalized therapy predictions without the need for any PDX engraftment in multiple solid tumors. *In situ* drug sensitivity screening could be a valuable clinical tool in personalizing treatment and stratifying patients in ovarian cancer and across solid tumor oncology.

Funding

National Cancer Institute Innovative Molecular Analysis Technologies program (R33 CA223904), Mayo Clinic-Koch Institute Cancer Solutions Team Grant, the Koch Institute Support (core) Grant P30-CA14051 from the National Cancer Institute, Dana-Farber/Harvard Cancer Center NCI Cancer Center Support Grant # NIH 5 P30 CA06516, Mayo Clinic Ovarian Cancer SPOR National Cancer Institute

P50 CA136393, National Cancer Institute R01 CA184502, and the National Science Foundation Graduate Research Fellowship Program under Grant No. (1122374).

CRediT authorship contribution statement

Max J. Cotler: Conceptualization, Investigation, Writing – review & editing, Formal analysis. **Khalil B. Ramadi:** Conceptualization, Investigation, Writing – review & editing, Formal analysis. **Xiaonan Hou:** Conceptualization, Investigation, Writing – review & editing, Formal analysis. **Elena Christodoulouopoulos:** Conceptualization, Investigation, Writing – review & editing, Formal analysis. **Sebastian Ahn:** Conceptualization, Investigation, Writing – review & editing, Formal analysis. **Ashvin Bashyam:** Software, Methodology, Writing – review & editing, Formal analysis. **Huiming Ding:** Software, Methodology, Writing – review & editing, Formal analysis. **Melissa Larson:** Software, Methodology, Writing – review & editing, Formal analysis. **Ann L. Oberg:** Software, Methodology, Writing – review & editing, Formal analysis. **Charles Whittaker:** Software, Methodology, Writing – review & editing, Formal analysis. **Oliver Jonas:** Writing – review & editing, Formal analysis. **Scott H. Kaufmann:** Writing – review & editing, Formal analysis. **S. John Weroha:** Writing – review & editing, Formal analysis. **Michael J. Cima:** Writing – review & editing, Formal analysis.

Declaration of Competing Interest

Kibur Medical, Inc. holds intellectual property related to this technology. Dr. Jonas has a financial interest in Kibur Medical. Data and materials availability: The data sets, materials, and analysis generated during the current study are available from the corresponding authors on reasonable request.

Acknowledgments

We thank P. Bursch, B. Miller, A. Lammers, K. Subramanyam, H. Montague-Alamin, M. Sherman, C. Frangieh, and all members of the Cima, Weroha, and Jonas Labs for technical discussions and support with this study. We thank B. Ferland and the Dana-Farber/Harvard Cancer Center in Boston, MA, for the use of the Specialized Histopathology Core and the Tissue Microarray Imaging Core, which provided histology, immunofluorescence, and imaging services. We also thank the Koch Institute Swanson Biotechnology Center's Hope Babette Tang (1983) Histology Facility (K. Cormier and C. Condon), Preclinical Imaging and Testing Core (M. Cornwall-Brady), and Barbara K. Ostrom (1978) Bioinformatics & Computing Facility (H. Ding and C. Whittaker). We also thank the women who donated their tumor tissue.

Supplementary materials

Supplementary material associated with this article can be found, in the online version, at [doi:10.1016/j.tranon.2022.101427](https://doi.org/10.1016/j.tranon.2022.101427).

References

- [1] K.T. Flaherty, R.J. Gray, A.P. Chen, S. Li, L.M. McShane, D. Patton, S.R. Hamilton, P. Mickey Williams, A. John Iafraite, J. Sklar, E.P. Mitchell, L.N. Harris, N. Takebe, D.J. Sims, B. Coffey, T. Fu, M. Routbort, J.A. Zwiebel, L.V. Rubinstein, R.F. Little, C.L. Arteaga, R. Comis, J.S. Abrams, P.J. O'Dwyer, B.A. Conley, Molecular landscape and actionable alterations in a genomically guided cancer clinical trial: National Cancer Institute molecular analysis for therapy choice (NCI-MATCH), *J. Clin. Oncol.* 38 (2020) 3883–3894, <https://doi.org/10.1200/JCO.19.03010>.
- [2] C. Robert, B. Karaszewska, J. Schachter, P. Rutkowski, A. Mackiewicz, D. Stroiakovski, M. Lichinitser, R. Dummer, F. Grange, L. Mortier, V. Chiarion-Sileni, K. Drucis, I. Krajsova, A. Hauschild, P. Lorigan, P. Wolter, G.V Long, K. Flaherty, P. Nathan, A. Ribas, A.-M. Martin, P. Sun, W. Crist, J. Legos, S. D. Rubin, S.M. Little, D. Schadendorf, Improved overall survival in melanoma with combined dabrafenib and trametinib, *N. Engl. J. Med.* 372 (2015) 30–39, <https://doi.org/10.1056/nejmoa1412690>.

- [3] A.K.S. Salama, S. Li, E.R. Macrae, J.-I. Park, E.P. Mitchell, J.A. Zwiebel, H.X. Chen, J.G. Robert, L.M. Mcshane, V.R. Larry, D. Patton, P. Mickey Williams, R.H. Stanley, D.K. Armstrong, B.A. Conley, L.A. Carlos, L.N. Harris, J.O.D. Peter, A.P. Chen, K. T. Flaherty, Dabrafenib and trametinib in patients with tumors with BRAF V600E mutations: results of the NCI-MATCH trial subprotocol H, *J. Clin. Oncol.* 38 (2020) 3895–3904, <https://doi.org/10.1200/JCO.20>.
- [4] J. Marquart, E.Y. Chen, V. Prasad, Estimation of the percentage of US patients with cancer who benefit from genome-driven oncology, *JAMA Oncol.* 4 (2018) 1093–1098, <https://doi.org/10.1001/jamaoncol.2018.1660>.
- [5] A. Haslam, J. Gill, V. Prasad, Estimation of the percentage of US patients with cancer who are eligible for immune checkpoint inhibitor drugs, *JAMA Netw. Open* 3 (2020), e200423, <https://doi.org/10.1001/jamanetworkopen.2020.0423>.
- [6] D. Schrag, H.S. Garewal, H.J. Burstein, D.J. Samson, D.D. Von Hoff, American Society of Clinical Oncology technology assessment: chemotherapy sensitivity and resistance assays somerfield for the ASCO Working Group on chemotherapy sensitivity and resistance assays, *J. Clin. Oncol.* 22 (2004) 3631–3638, <https://doi.org/10.1200/JCO.2004.05.065>.
- [7] R.L. Siegel, K.D. Miller, A. Jemal, Cancer statistics, 2020, *CA Cancer J. Clin.* 70 (2020) 7–30, <https://doi.org/10.3322/caac.21590>.
- [8] F. Muggia, Recent updates in the clinical use of platinum compounds for the treatment of gynecologic cancers, *Semin. Oncol.* 31 (2004) 17–24.
- [9] R. Ozols, Systemic therapy for ovarian cancer: current status and new treatments, *Semin. Oncol.* 33 (2006) S3–11.
- [10] A. du Bois, J. Pfisterer, Future options for first-line therapy of advanced ovarian cancer, *Int. J. Gynecol. Cancer* 15 (2005) 42–50, <https://doi.org/10.1111/j.1525-1438.2005.15356.x>.
- [11] G.D. Aletti, S.C. Dowdy, B.S. Gostout, M.B. Jones, R.C. Stanhope, T.O. Wilson, K. C. Podratz, W.A. Cliby, Quality improvement in the surgical approach to advanced ovarian cancer: the mayo clinic experience, *ACS 208* (2009) 614–620, <https://doi.org/10.1016/j.jamcollurg.2009.01.006>.
- [12] G.D. Aletti, E.L. Eisenhauer, A. Santillan, A. Axtell, G. Aletti, C. Holschneider, D. S. Chi, R.E. Bristow, W.A. Cliby, Identification of patient groups at highest risk from traditional approach to ovarian cancer treatment, *Gynecol. Oncol.* 120 (2011) 23–28, <https://doi.org/10.1016/j.ygyno.2010.09.010>.
- [13] K. Bell-McGuinn, J. Konner, W. Tew, D.R. Spriggs, New drugs for ovarian cancer, *Ann. Oncol.* 22 (2011) 77–82, <https://doi.org/10.1093/annonc/mdr531>.
- [14] S. Vaughan, J.I. Coward, R.C. Bast, A. Berchuck, J.S. Berek, J.D. Brenton, G. Coukos, C.C. Crum, R. Drapkin, D. Etemadmoghadam, M. Friedlander, H. Gabra, S.B. Kaye, C.J. Lord, E. Lengyel, D.A. Levine, I.A. McNeish, U. Menon, G.B. Mills, K. P. Nephew, A.M. Oza, A.K. Sood, E.A. Stronach, H. Walczak, D.D. Bowtell, F. R. Balkwill, Rethinking ovarian cancer: recommendations for improving outcomes, *Nat. Rev. Cancer* 11 (2011) 719–725, <https://doi.org/10.1038/nrc3144>.
- [15] P.E. Colombo, M. Fabbro, C. Theillet, F. Bibeau, P. Rouanet, I. Ray-Coquard, Sensitivity and resistance to treatment in the primary management of epithelial ovarian cancer, *Crit. Rev. Oncol.* 89 (2014) 207–216, <https://doi.org/10.1016/j.critrevonc.2013.08.017>.
- [16] B. Oronsky, C.M. Ray, A.I. Spira, J.B. Trepel, C.A. Carter, H.M. Cottrill, A brief review of the management of platinum-resistant–platinum-refractory ovarian cancer, *Med. Oncol.* 34 (2017) 1–7, <https://doi.org/10.1007/s12032-017-0960-z>.
- [17] G.C. Jayson, E.C. Kohn, H.C. Kitchener, J.A. Ledermann, Ovarian cancer, *Lancet* 384 (2014) 1376–1388, [https://doi.org/10.1016/S0140-6736\(13\)62146-7](https://doi.org/10.1016/S0140-6736(13)62146-7).
- [18] D. Bell, A. Berchuck, M. Birrer, J. Chien, D.W. Cramer, F. Dao, R. Dhir, P. Disaia, H. Gabra, P. Glenn, A.K. Godwin, J. Gross, L. Hartmann, M. Huang, D. G. Huntsman, M. Iacocca, M. Imielinski, S. Kalloger, B.Y. Karlan, D.A. Levine, G. B. Mills, C. Morrison, D. Mutch, N. Olvera, S. Orsulic, K. Park, N. Petrelli, B. Rabeno, J.S. Rader, B.I. Sikic, K. Smith-McCune, A.K. Sood, D. Bowtell, R. Penny, J.R. Testa, K. Chang, H.H. Dinh, J.A. Drummond, G. Fowler, P. Gunaratne, A. C. Hawes, C.L. Kovar, L.R. Lewis, M.B. Morgan, I.F. Newsham, J. Santibanez, J. G. Reid, L.R. Trevino, Y.Q. Wu, M. Wang, D.M. Muzny, D.A. Wheeler, R.A. Gibbs, G. Getz, M.S. Lawrence, K. Cibulskis, A.Y. Sivachenko, C. Sougnez, D. Voet, J. Wilkinson, T. Bloom, K. Ardlie, T. Fennell, J. Baldwin, S. Gabriel, E.S. Lander, L. Ding, R.S. Fulton, D.C. Koboldt, M.D. McLellan, T. Wylie, J. Walker, M.O. Laughlin, D.J. Dooling, L. Fulton, R. Abbott, N.D. Dees, Q. Zhang, C. Kandoth, M. Wendl, W. Schierding, D. Shen, C.C. Harris, H. Schmidt, J. Kalicki, K. D. Delehaunty, C.C. Fronick, R. Demeter, L. Cook, J.W. Wallis, L. Lin, V.J. Magrini, J.S. Hodges, J.M. Eldred, S.M. Smith, C.S. Pohl, F. Vandin, B.J. Raphael, G. M. Weinstock, E.R. Mardis, R.K. Wilson, M. Meyerson, W. Winckler, R.G. W. Verhaak, S.L. Carter, C.H. Mermel, G. Saksena, H. Nguyen, R.C. Onofrio, D. Hubbard, S. Gupta, A. Crenshaw, A.H. Ramos, L. Chin, A. Protopopov, J. Zhang, T.M. Kim, I. Perna, Y. Xiao, H. Zhang, G. Ren, N. Sathiamoorthy, R.W. Park, E. Lee, P.J. Park, R. Kucherlapati, D.M. Absher, L. Waite, G. Sherlock, J.D. Brooks, J.Z. Li, J. Xu, R.M. Myers, P.W. Laird, L. Cope, J.G. Herman, H. Shen, D.J. Weisenberger, H. Nouchmeh, F. Pan, T. Triche, B.P. Berman, D.J. Van Den Berg, J. Buckley, S. B. Bayliss, P.T. Spellman, E. Purdom, P. Neuvial, H. Bengtsson, L.R. Jakkula, S. Durinck, J. Han, S. Dorton, H. Marr, Y. Choi, V. Wang, N.J. Wang, J. Ngai, J. G. Conboy, B. Parvin, H.S. Feiler, T.P. Speed, J.W. Gray, N.D. Socci, Y. Liang, B. S. Taylor, N. Schultz, L. Borsu, A.E. Lash, C. Brennan, A. Viale, C. Sander, M. Ladanyi, K.A. Hoadley, S. Meng, Y. Du, Y. Shi, L. Li, Y.J. Turman, D. Zang, E. B. Helms, S. Balu, X. Zhou, J. Wu, M.D. Topal, D.N. Hayes, C.M. Perou, C.J. Wu, S. Shukla, A. Sivachenko, R. Jing, Y. Liu, M. Noble, H. Carter, D. Kim, R. Karchin, J. E. Korkola, L.M. Heiser, R.J. Cho, Z. Hu, E. Cerami, A. Olshen, B. Reva, Y. Antipin, R. Shen, P. Mankoo, R. Sheridan, G. Ciriello, W.K. Chang, J.A. Bermanke, D. Haussler, C.C. Benz, J.M. Stuart, S.C. Benz, J.Z. Sanborn, C.J. Vaske, J. Zhu, C. Szeto, G.K. Scott, C. Yau, M.D. Wilkerson, N. Zhang, R. Akbani, K.A. Baggerly, W.K. Yung, J.N. Weinstein, T. Shelton, D. Grimm, M. Hatfield, S. Morris, P. Yena, P. Rhodes, M. Sherman, J. Paulauskis, S. Millis, A. Kahn, J.M. Greene, R. Sfeir, M. A. Jensen, J. Chen, J. Whitmore, S. Alonso, J. Jordan, A. Chu, A. Barker, C. Compton, G. Eley, M. Ferguson, P. Fielding, D.S. Gerhard, R. Myles, C. Schaefer, K.R. Mills Shaw, J. Vaught, J.B. Vockley, P.J. Good, M.S. Guyer, B. Ozenberger, J. Peterson, E. Thomson, Integrated genomic analyses of ovarian carcinoma, *Nature* 474 (2011) 609–615, <https://doi.org/10.1038/nature10166>.
- [19] C. Tian, K.R. Clauser, D. Öhlund, S. Rickelt, Y. Huang, M. Gupta, D.R. Mani, S. A. Carr, D.A. Tuveson, R.O. Hynes, Proteomic analyses of ECM during pancreatic ductal adenocarcinoma progression reveal different contributions by tumor and stromal cells, *Proc. Natl. Acad. Sci. U. S. A.* 116 (2019) 19609–19618, <https://doi.org/10.1073/pnas.1908626116>.
- [20] D. Hanahan, R.A. Weinberg, Leading edge review hallmarks of cancer: the next generation, (n.d.). 10.1016/j.cell.2011.02.013.
- [21] N. Iida, A. Dzutsev, C.A. Stewart, L. Smith, N. Bouladoux, R.A. Weingarten, D. A. Molina, R. Salcedo, T. Back, S. Cramer, R.M. Dai, H. Kiu, M. Cardone, S. Naik, A. K. Patri, E. Wang, F.M. Marincola, K.M. Frank, Y. Belkaid, G. Trinchieri, R. S. Goldszmid, Commensal bacteria control cancer response to therapy by modulating the tumor microenvironment, *Science* 342 (2013) 967–970, <https://doi.org/10.1126/science.1240527> (80-).
- [22] J. Lee, D.H. Jo, J.H. Kim, C.S. Cho, J.E. Han, Y. Kim, H. Park, S.H. Yoo, Y.S. Yu, H. E. Moon, H.R. Park, D.G. Kim, J.H. Kim, S.H. Paek, Development of a patient-derived xenograft model of glioblastoma via intravitreal injection in mice, *Exp. Mol. Med.* 51 (2019), <https://doi.org/10.1038/s12276-019-0241-3>.
- [23] L.E. Dobrolecki, S.D. Airhart, D.G. Alferetz, S. Aparicio, F. Behbod, M. Bentires-Alj, C. Briskin, C.J. Bult, S. Cai, R.B. Clarke, H. Dowst, M.J. Ellis, E. Gonzalez-Suarez, R. D. Iggo, P. Kabos, S. Li, G.J. Lindeman, E. Marangoni, A. McCoy, F. Meric-Bernstam, H. Piwnica-Worms, M.F. Poupon, J. Reis-Filho, C.A. Sartorius, V. Scabia, G. Sflomos, Y. Tu, F. Vaillant, J.E. Visvader, A. Welm, M.S. Wicha, M.T. Lewis, Patient-derived xenograft (PDX) models in basic and translational breast cancer research, *Cancer Metastasis Rev.* 35 (2016) 547–573, <https://doi.org/10.1007/s10555-016-9653-x>.
- [24] S. Okada, K. Vaeteewoontacharn, R. Kariya, Establishment of a patient-derived tumor xenograft model and application for precision cancer medicine, *Chem. Pharm. Bull.* 66 (2018) 225–230, <https://doi.org/10.1248/cpb.c17-00789>.
- [25] E.B. Jo, D. Hong, Y.S. Lee, H. Lee, J.B. Park, S.J. Kim, Establishment of a novel PDX mouse model and evaluation of the tumor suppression efficacy of bortezomib against liposarcoma, *Transl. Oncol.* (2019), <https://doi.org/10.1016/j.tranon.2018.09.015>.
- [26] G. Bondarenko, A. Ugolkov, S. Rohan, P. Kulesza, O. Dubrovskiy, D. Gursel, J. Mathews, T.V. O'Halloran, J.J. Wei, A.P. Mazar, Patient-derived tumor xenografts are susceptible to formation of human lymphocytic tumors, *Neoplasia* 17 (2015) 735–741, <https://doi.org/10.1016/j.neo.2015.09.004>.
- [27] S.J. Weroha, M.A. Becker, S. Enderica-Gonzalez, S.C. Harrington, A.L. Oberg, M. J. Maurer, S.E. Perkins, M. AlHilli, K.A. Butler, S. McKinstry, S. Fink, R.B. Jenkins, X. Hou, K.R. Kalli, K.M. Goodman, J.N. Sarkaria, B.Y. Karlan, A. Kumar, S. H. Kaufmann, L.C. Hartmann, P. Haluska, Tumorgrafts as *in vivo* surrogates for women with ovarian cancer, *Clin. Cancer Res.* 20 (2014) 1288–1297, <https://doi.org/10.1158/1078-0432.CCR-13-2611>.
- [28] G. Glaser, S.J. Weroha, M.A. Becker, X. Hou, S. Enderica-Gonzalez, S.C. Harrington, P. Haluska, Conventional chemotherapy and oncogenic pathway targeting in ovarian carcinosarcoma using a patient-derived tumorgraft, *PLoS One* 10 (2015), e0126867, <https://doi.org/10.1371/journal.pone.0126867>.
- [29] K.A. Butler, X. Hou, M.A. Becker, V. Zanfagnin, S. Enderica-Gonzalez, D. Visscher, K.R. Kalli, P. Tienchaianada, P. Haluska, S.J. Weroha, Prevention of human lymphoproliferative tumor formation in ovarian cancer patient-derived xenografts, *Neoplasia* 19 (2017) 628–636, <https://doi.org/10.1016/j.neo.2017.04.007> (United States).
- [30] Y. Liu, P. Chanana, J.I. Davila, X. Hou, V. Zanfagnin, C.D. McGehee, E.L. Goode, E. C. Polley, P. Haluska, S.J. Weroha, C. Wang, Gene expression differences between matched pairs of ovarian cancer patient tumors and patient-derived xenografts, *Sci. Rep.* 9 (2019), <https://doi.org/10.1038/s41598-019-42680-2>.
- [31] M.M. Alhilli, M.A. Becker, S.J. Weroha, K.S. Flatten, R.M. Hurley, M.I. Harrell, A. L. Oberg, M.J. Maurer, K.M. Hawthorne, X. Hou, S.C. Harrington, S. McKinstry, X. W. Meng, K.M. Wilcoxon, K.R. Kalli, E.M. Swisher, S.H. Kaufmann, P. Haluska, T. Merck, G.O. Author, *In vivo* anti-tumor activity of the PARP inhibitor niraparib in homologous recombination deficient and proficient ovarian carcinoma ☆☆☆ HHS public access author manuscript, *Gynecol. Oncol.* 143 (2016) 379–388, <https://doi.org/10.1016/j.ygyno.2016.08.328>.
- [32] O. Jonas, H.M. Landry, J.E. Fuller, J.T. Santini, J. Baselga, R.H.I. Tepper, M.J. Cima, R. Langer, An implantable microdevice to perform high-throughput *in vivo* drug sensitivity testing in tumors, *Sci. Transl. Med.* 7 (2015) 284ra57, <https://doi.org/10.1126/scitranslmed.3010564>.
- [33] O. Jonas, M.J. Oudin, T. Kosciuk, M. Whitman, F.B. Gertler, M.J. Cima, K. T. Flaherty, R. Langer, Parallel *in vivo* assessment of drug phenotypes at various time points during systemic BRAF inhibition reveals tumor adaptation and altered treatment vulnerabilities, *Clin. Cancer Res.* 22 (2016) 6031–6038, <https://doi.org/10.1158/1078-0432.CCR-15-2722>.
- [34] Y. Zwang, O. Jonas, C. Chen, M.L. Rinne, J.G. Doench, F. Piccioni, L. Tan, H. T. Huang, J. Wang, Y.J. Ham, J. O'Connell, P. Bhola, M. Doshi, M. Whitman, M. Cima, A. Letai, D.E. Root, R.S. Langer, N. Gray, W.C. Hahn, Synergistic interactions with PI3K inhibition that induce apoptosis, *Elife* 6 (2017) 1–18, <https://doi.org/10.7554/eLife.24523>.
- [35] O. Jonas, J.W. Kang, S.P. Singh, A. Lammers, F.T. Nguyen, R.R. Dasari, P.T.C. So, R. Langer, M.J. Cima, *In vivo* detection of drug-induced apoptosis in tumors using Raman spectroscopy, *Analyst* 143 (2018) 4836–4839, <https://doi.org/10.1039/c8an00913a>.

- [36] S.K. Bhagavatula, K. Upadhyaya, B.J. Miller, P. Bursch, A. Lammers, M.J. Cima, S. G. Silverman, O. Jonas, An interventional image-guided microdevice implantation and retrieval method for *in-vivo* drug response assessment, *Med. Phys.* 46 (2019) 5134–5143, <https://doi.org/10.1002/mp.13803>.
- [37] R.A. Klinghoffer, S.B. Bahrami, B.A. Hatton, J.P. Frazier, A. Moreno-Gonzalez, A. D. Strand, W.S. Kerwin, J.R. Casalini, D.J. Thirstrup, S. You, S.M. Morris, K. L. Watts, M. Veisoh, M.O. Grenley, I. Tretyak, J. Dey, M. Carleton, E. Beirne, K. D. Pedro, S.H. Ditzler, E.J. Girard, T.L. Deckwerth, J.A. Bertout, K.A. Meleo, E. H. Filvaroff, R. Chopra, O.W. Press, J.M. Olson, A technology platform to assess multiple cancer agents simultaneously within a patient's tumor, *Sci. Transl. Med.* 7 (2015) 284ra56, <https://doi.org/10.1126/scitranslmed.aaa7489>.
- [38] K.R. Gundle, G.B. Deutsch, H.J. Goodman, S.M. Pollack, M.J. Thompson, J. L. Davis, M.Y. Lee, D.C. Ramirez, W. Kerwin, J.A. Bertout, M.O. Grenley, K.H. W. Sottero, E. Beirne, J. Frazier, J. Dey, M. Ellison, R.A. Klinghoffer, R.G. Maki, Multiplexed evaluation of microdosed antineoplastic agents *in situ* in the tumor microenvironment of patients with soft tissue sarcoma, *Clin. Cancer Res.* 26 (2020) 3958–3968, <https://doi.org/10.1158/1078-0432.CCR-20-0614>.
- [39] D.F. Heitjan, A. Manni, R.J. Santen, Statistical analysis of *in vivo* tumor growth experiments1, 1993.
- [40] W.W. Stroup, G.A. Milliken, E.A. Claassen, R.D. Wolfinger, *SAS for Mixed Models: Introduction and Basic Applications*, SAS Institute, Cary, NC, 2018.
- [41] A.L. Oberg, E.P. Heinzen, X. Hou, M.M. Al Hilli, R.M. Hurley, A.E. Wahner Hendrickson, K.M. Goergen, M.C. Larson, M.A. Becker, J.E. Eckel-Passow, M. J. Maurer, S.H. Kaufmann, P. Haluska, S.J. Weroha, Statistical analysis of comparative tumor growth repeated measures experiments in the ovarian cancer patient derived xenograft (PDX) setting, *Sci. Rep.* 11 (2021) 8076, <https://doi.org/10.1038/s41598-021-87470-x>.
- [42] F. Pedregosa FABIANPEDREGOSA, V. Michel, O. Grisel OLIVIERGRISEL, M. Blondel, P. Prettenhofer, R. Weiss, J. Vanderplas, D. Cournapeau, F. Pedregosa, G. Varoquaux, A. Gramfort, B. Thirion, O. Grisel, V. Dubourg, A. Passos, M. Brucher, M. Perrot andÉdouardand, andÉdouard Duchesnay, Fré. Duchesnay EDOUARDUCHESNAY, Scikit-learn: machine learning in Python Gaël Varoquaux Bertrand Thirion Vincent Dubourg Alexandre Passos PEDREGOSA, VAROQUAUX, GRAMFORT ET AL. Matthieu Perrot, 2011.
- [43] K.C. Li, Asymptotic optimality for \mathcal{L}_p , \mathcal{L}_q cross-validation and generalized cross-validation: discrete index set, *Ann. Stat.* 15 (1987) 958–975, <https://doi.org/10.1214/aos/1176350486>.
- [44] Y. Yang, Consistency of cross validation for comparing regression procedures, *Ann. Stat.* 35 (2007) 2450–2473, <https://doi.org/10.1214/009053607000000514>.
- [45] J. Shao, Linear model selection by cross-validation, *J. Am. Stat. Assoc.* 88 (1993) 486–494, <https://doi.org/10.1080/01621459.1993.10476299>.
- [46] K.C. Bible, S.H. Kaufmann, Flavopiridol: a cytotoxic flavone that induces cell death in noncycling A549 human lung carcinoma cells, *Cancer Res.* 56 (1996) 4856–4861.
- [47] P.F. McAuliffe, K.W. Evans, A. Akcakanat, K. Chen, X. Zheng, H. Zhao, A. K. Eterovic, T. Sangai, A.M. Holder, C. Sharma, H. Chen, K.A. Do, E. Tarco, M. Gagea, K.A. Naff, A. Sahin, A.S. Multani, D.M. Black, E.A. Mittendorf, I. Bedrosian, G.B. Mills, A.M. Gonzalez-Angulo, F. Meric-Bernstam, Ability to generate patient-derived breast cancer xenografts is enhanced in chemoresistant disease and predicts poor patient outcomes, *PLoS One* 10 (2015) 1–20, <https://doi.org/10.1371/journal.pone.0136851>.
- [48] P.F. McAuliffe, K.W. Evans, A. Akcakanat, K. Chen, X. Zheng, H. Zhao, A. K. Eterovic, T. Sangai, A.M. Holder, C. Sharma, H. Chen, K.A. Do, E. Tarco, M. Gagea, K.A. Naff, A. Sahin, A.S. Multani, D.M. Black, E.A. Mittendorf, I. Bedrosian, G.B. Mills, A.M. Gonzalez-Angulo, F. Meric-Bernstam, Erratum: ability to generate patient-derived breast cancer xenografts is enhanced in chemoresistant disease and predicts poor patient outcomes (PLoS ONE (2015) 10:9 (e0136851) DOI: 10.1371/journal.pone.0136851), *PLoS One* 11 (2016) 8–9, <https://doi.org/10.1371/journal.pone.0151121>.
- [49] E. Marangoni, A. Vincent-Salomon, N. Auger, A. Degeorges, F. Assayag, P. De Cremoux, L. De Plater, C. Guyader, G. De Pinieux, J.G. Judde, M. Rebutti, C. Tran-Perennou, X. Sastre-Garau, B. Sigal-Zafrani, O. Delattre, V. Diéras, M.F. Poupon, A new model of patient tumor-derived breast cancer xenografts for preclinical assays, *Clin. Cancer Res.* 13 (2007) 3989–3998, <https://doi.org/10.1158/1078-0432.CCR-07-0078>.